

# Chapter 2

## Multi-level Image Thresholding Based on Hybrid Differential Evolution Algorithm. Application on Medical Images

M. Ali, P. Siarry and M. Pant

### 2.1 Introduction

Image thresholding is definitely one of the most popular segmentation approaches for extracting objects from the background, or for discriminating objects from objects that have distinct gray-levels. It is typically simple and computationally efficient. It is based on the assumption that the objects can be distinguished by their gray levels. The optimal threshold is the one that can separate different objects from each other or from the background to such an extent that a decision can be made without further processing [8, 13]. The automatic fitting of this threshold is one of the main challenges of image segmentation. Sezgin and Sankur [18] have presented a survey of a variety of thresholding techniques. There are a lot of approaches classifying thresholding methods. Authors in [18] labeled the method according to the information they exploit, such as histogram shape, space measurement clustering, entropy, object attributes, spatial information and local gray-level surface. Another classification approach consists in dividing these techniques into parametric and non-parametric techniques. The parametric thresholding methods exploit the first-order statistical characterization of the image to be segmented. Weszka et al. [16] proposed a parametric method where the gray-level distribution of each class is assumed to be a Gaussian distribution. An attempt to find an estimate of the parameters of the distribution that best fit the given histogram data is made by using the least-squares estimation method. Typically, it leads to a nonlinear optimization problem, its solution is computationally expensive and time consuming. Over the years, many researchers have proposed several algorithms to solve the objective function of Gaussian curve fitting for multi-level

---

M. Ali · M. Pant

Department of Paper Technology, Indian Institute of Technology Roorkee,  
Roorkee 247667, India

P. Siarry (✉)

Laboratory of LISSI, Université Paris Est, Champs-sur-Marne, France  
e-mail: siarry@u-pec.fr

thresholding. For example, Snyder et al. [10] presented an alternative method for fitting curves based on a heuristic method called tree annealing; Nakib et al. [11, 19] proposed a fast scheme for optimal thresholding using a simulated annealing algorithm; Zahara et al. [7] proposed a hybrid Nelder–Mead Particle Swarm Optimization (NM-PSO) method. More recently a hybrid method based on Expectation Maximization (EM) and Particle Swarm Optimization (PSO+EM) is proposed in [14] and the application of basic Differential Evolution (DE) for solving image segmentation problem is shown in [6], and recently in [2]. Moreover, the application of the artificial bees algorithm can be found in [3]. All these metaheuristic based methods are efficient in solving the multi-level thresholding problem and could provide better effectiveness than the other traditional methods (local search and deterministic methods). However, curve fitting is usually time-consuming which indicates that improved methods are needed to enhance the efficiency of existing methods while maintaining quality effectiveness. Further, these methods also have many parameters that must be well fitted. In the present study we have analyzed whether the thresholding techniques can be further improved if we use a modified variant of DE. In the recent years DE [15] [17] has gained much popularity in different kind of applications because of its simplicity and robustness in comparison to other evolutionary algorithms [17]. DE has very few parameters to adjust, making it particularly easy to implement to a diverse set of optimization problems [1, 5, 9]. This paper proposes the development of a new optimal multilevel thresholding algorithm based on image histograms by employing its improved version called Hybrid Differential Evolution (HDE). After fitting the Gaussian curves using HDE, optimal threshold is calculated by minimizing the overall probability error between these Gaussian distributions. The paper is outlined as follows. Section 2.2 introduces the procedure of Gaussian curve fitting. In Sect. 2.3, the overall probability of error for finding optimal thresholds from fitted Gaussian curves is described. Section 2.4, presents enhanced differential evolution version. Section 2.5 provides the experimental results and discussions, while Sect. 2.6 concludes this research.

## 2.2 Gaussian Curve Fitting

A properly normalized multimodal histogram  $h(x)$  of an image  $I$ , where  $x \in [0, L - 1]$  represents the gray levels and, and  $L$  is the total number of gray levels, can be fitted with the sum of  $d$  probability density functions (pdf's) for finding the optimal thresholds for use in image segmentation [10]. The case where the Gaussian pdf's are used is defined by:

$$p(x) = \sum_{i=1}^d P_i \exp \left[ -\frac{(x - \mu_i)^2}{\sigma_i^2} \right] \quad (2.1)$$

where  $P_i$  is the amplitude of the Gaussian pdf,  $\mu_i$  is the mean and  $\sigma_i^2$  is the variance respectively, of mode  $i$  and  $d$  is number of Gaussians used to approximate the original histogram and corresponds to the number of the segmentation classes. A pdf model must be fitted to the histogram data, typically by using the maximum likelihood or mean-squared error approach, in order to locate the optimal threshold. Given the histogram data  $h(j)$  (observed probability of gray level  $j$ ), it can be defined as follows:

$$h(j) = \frac{g(j)}{\sum_{i=0}^d g(i)} \quad (2.2)$$

where  $g(j)$  denotes the occurrence of gray-level  $j$  over a given image ranges  $[0, L - 1]$ . Our goal is to find a set of parameters,  $\Theta$ , that minimizes the fitting error  $J$ , given by the following expression [11, 19]:

$$\underset{\Theta}{Min} J = \frac{\sum_i |h(i) - p(\Theta, x_i)|}{\sum_i h(i)} \quad (2.3)$$

where  $i$  ranges over the bins in the measured histogram. Here,  $J$  is the objective function to be minimized with respect to, a set of parameters defining the Gaussian pdfs and the probabilities, is given by:

$$\Theta = \{P_i, \mu_i, \sigma_i\} \quad (2.4)$$

The standard process of setting the partial derivatives to zero results in a set of non-linear coupled equations, the system usually being solved through numerical techniques.

### 2.3 Overall Probability of Error

After fitting the multimodal histogram, the optimal threshold could be determined by minimizing the overall probability of error, for two adjacent Gaussian pdfs, given by

$$e(T_i) = P_i \int_{-\infty}^{T_i} p_i(x) dx + P_{i+1} \int_{T_i}^{\infty} p_{i+1}(x) dx \quad (2.5)$$

with respect to the threshold  $T_i$ , where  $p_i(x)$  is the  $i$ th pdf [8]. Then the overall probability to minimize is:

$$E(T) = \sum_{i=1}^{d-1} e(T_i) \quad (2.6)$$

where  $T$  is the vector of thresholds:  $0 < T_1 < T_2 < \dots < T_{d-1} < L - 1$ . In our case  $L$  is equal to 256

To find the thresholds values for which this error is minimal requires differentiating  $e(T_i)$  with respect to  $T_i$  (using Leibniz's rule) and equating the result to zero. It gives:

$$P_i \times p_i(T_i) = P_{i+1} \times p_{i+1}(T_i) \quad (2.7)$$

This equation is solved for  $T_i$  to find the optimum threshold. Using Eq. 2.1 in the general solution of Eq. 9.6 results in the following solution for the threshold  $T_i$ :

$$AT_i^2 + BT_i + C = 0 \quad (2.8)$$

where:

$$\begin{aligned} A &= \sigma_i^2 - \sigma_{i+1}^2 \\ B &= 2 \times (\mu_i \sigma_{i+1}^2 - \mu_{i+1} \sigma_i^2) \\ C &= \mu_{i+1}^2 \sigma_i^2 - \mu_i^2 \sigma_{i+1}^2 + 4\sigma_i^2 \sigma_{i+1}^2 \log \left( \frac{P_i \sigma_{i+1}^2}{P_{i+1} \sigma_i^2} \right) \end{aligned}$$

Since a quadratic equation has two possible solutions, only one of them is a feasible solution [6].

## 2.4 Hybrid Differential Evolution (HDE)

In this section we briefly describe HDE, an enhanced version of basic DE. HDE uses the concepts of opposition based learning, random localization and has a one population set structure. The working of HDE is as follows. *Population initialization*: HDE starts with a population  $S = \{X_1, X_2, \dots, X_{NP}\}$  of  $NP$  solutions:  $X_i = (x_{1,i}, \dots, x_{NP,i})$ , where the index  $i$  denotes the  $i^{th}$  solution of the population. For this we randomly construct a population  $P_1$  of  $NP$  solutions, using the following rule:

$$x_{i,j} = x_{\min,j} + \text{Sob}(0, 1) \times (x_{\max,j} - x_{\min,j}) \quad (2.9)$$

where  $x_{\min,j}$  and  $x_{\max,j}$  are lower and upper bounds respectively, for  $j^{th}$  component, respectively.  $\text{Sob}(0, 1)$  is a number between 0 and 1 from a low discrepancy sequence generated using Sobol's method [4].

We construct another population  $P_2$  of  $NP$  opposite solutions to the solutions in population  $P_1$  using the following rule:

$$y_{i,j} = x_{\min,j} + x_{\max,j} - x_{i,j} \quad (2.10)$$

where  $x_{i,j}$  is the component of solution  $X_i$  of the population  $P_1$ .

Now the initial population  $S$  is constructed by taking the  $NP$  best solutions from union of  $P_1$  and  $P_2$ .

*Mutation:* The mutation operation of HDE applies the vector difference between the existing population members for determining both the degree and direction of perturbation applied to the individual subject of the mutation operation.

The mutation process at each generation begins by randomly selecting three solutions  $X_{r1}$ ,  $X_{r2}$ ,  $X_{r3}$  from the population corresponding to target solution  $X_i$ .

Unlike DE, HDE holds a tournament between the three solutions and the region around the best point is explored. That is to say if  $X_{r1}$  is the point having the best fitness function value then the region around it is searched with the hope of getting a better solution. Assuming that  $X_{tb} = X_{r1}$ , the mutation equation is given as:

$$V_i = X_{tb} + F \times (X_{r2} - X_{r3}) \quad (2.11)$$

where  $r1, r2, r3 \in 1, \dots, NP$  are randomly selected such that  $r1 \neq r2 \neq r3 \neq i$ , and  $F$  is the control parameter such that  $F \in [0, 1]$ .

This variation gradually transforms itself into a search intensification feature for rapid convergence once the points in  $S$  form a cluster around the global minima.

*The Crossover:* crossover operator of HDE is same as of DE. According to it, once the perturbed individual  $V_i = (v_{i,j}, \dots, v_{n,i})$  is generated, it is subjected to a crossover operation with the target individual  $X_i = (x_{1,i}, \dots, x_{n,i})$ , that finally generates the trial solution,  $U_i = (u_{1,i}, \dots, u_{n,i})$ , as follows:

$$u_{ij} = \begin{cases} v_{i,j} & \text{if } rand_j \leq C_r \text{ or } j = k \\ x_{i,j} & \text{Otherwise} \end{cases} \quad (2.12)$$

where,  $j = 1, \dots, n$  and  $k1, \dots, n$  is a random parameters index, chosen once for each  $i$ . The crossover rate,  $C_r \in [0, 1]$ , is set by the user.

*Selection:* The selection operator used in HDE is same as that of the classical DE, but the method of updating the solutions differs from that of it. After generation of new solution a selection operation is performed between it and its corresponding target solution by the following equation:

$$X'_i = \begin{cases} U_i & \text{if } f(U_i) \leq f(X_i) \\ X_i & \text{Otherwise} \end{cases} \quad (2.13)$$

If new solution is better than target solution then it replaces target solution in current population. This is in contrast to basic DE, where, the better one of the two is added to an auxiliary population. In DE, two populations (current and auxiliary) are considered simultaneously in all the iterations that result in the consumption of extra memory and CPU time. On the other hand in HDE, only one population is maintained and the individuals are updated when a better solution is found. Also, the

newly found better solution that enters the population instantly becomes a variable to take part in the creation of new solution.

## 2.5 Experimental Results

In this section, we evaluate the performance of the algorithm while implementing Gaussian curve fitting for multi-level thresholding. The test images Sailboat is of size  $512 \times 512$ , Cameraman and Lena, are of size pixels with 8 bit gray-levels, taken under natural lighting without the support of any special light source. Test images and their respective normalized histograms are given in Fig. 2.1. The algorithm is implemented on a 2.4 GHz Intel Core i5 Macbook pro with 4GB RAM using Matlab R2013a. The stopping criterion we used for the algorithm is the maximum number of iteration. HDE has only 4 parameters that must be well fitted. We have done preliminary testing for the purpose of getting suitable values of these parameters and the fine tuned results are listed in Table 2.1. The parameters  $P_i$ ,  $\mu_i$  and  $\Sigma_i$  are randomly initialized along with some restrictions to each parameter (for example  $P_i$  must be between 0 and 1,  $\mu_i$  must be between 0 and 255).

The experimental results are listed in Table 2.2. This shows the number of classes, parameters of Gaussian curves, the threshold values and the CPU time achieved by the proposed method. The CPU times recorded do not include computation times of the threshold values. Figures 2.2, 2.3, 2.4, 2.5, 2.6 and 2.7 show the results of individual Gaussian curves, fitting to a sum of Gaussian curves to the histograms of the images of Fig. 2.1, and their corresponding segmented images, respectively.

We have conducted two experiments with every image. Experiments on images Cameraman and Sailboat are performed taking three and four classes while in the case of Lena it is three and five. The layout in Figs. 2.2b, 2.3b, 2.4b, 2.5b, 2.6b and 2.7b suggests an easy combination of the Gaussian functions which approaches to shape of the histogram of the original image. Figures 2.2c, 2.3c, 2.4c, 2.5c, 2.6c and 2.7c show the segmented image, in these cases thresholds values are calculated according to (2.7). It is evident that the resulting function approaches the original histogram in all the cases.

In the above experiment, the number of iterations, which is used as stopping criterion, was fixed and corresponding results are noted. However, in order to compare the convergence time of HDE algorithm with basic DE, we have computed the number of function evaluations (NFEs) and the corresponding CPU time for both the algorithms. The run of each algorithm was stopped when the fitting error  $J$  of the best solution reached  $\varepsilon$ . i.e.  $\min f \leq \varepsilon = 10^{-1}$ , where  $\varepsilon$  is a threshold value which fixes the accuracy of the measurement. Therefore, the stopping criterion is modified; it is based on the value of the fitting and not on the number of iterations. Table 2.3 gives the NFEs and the CPU time taken by each algorithm to meet the stopping criteria. From this Table we can clearly see the competitive performance of HDE.

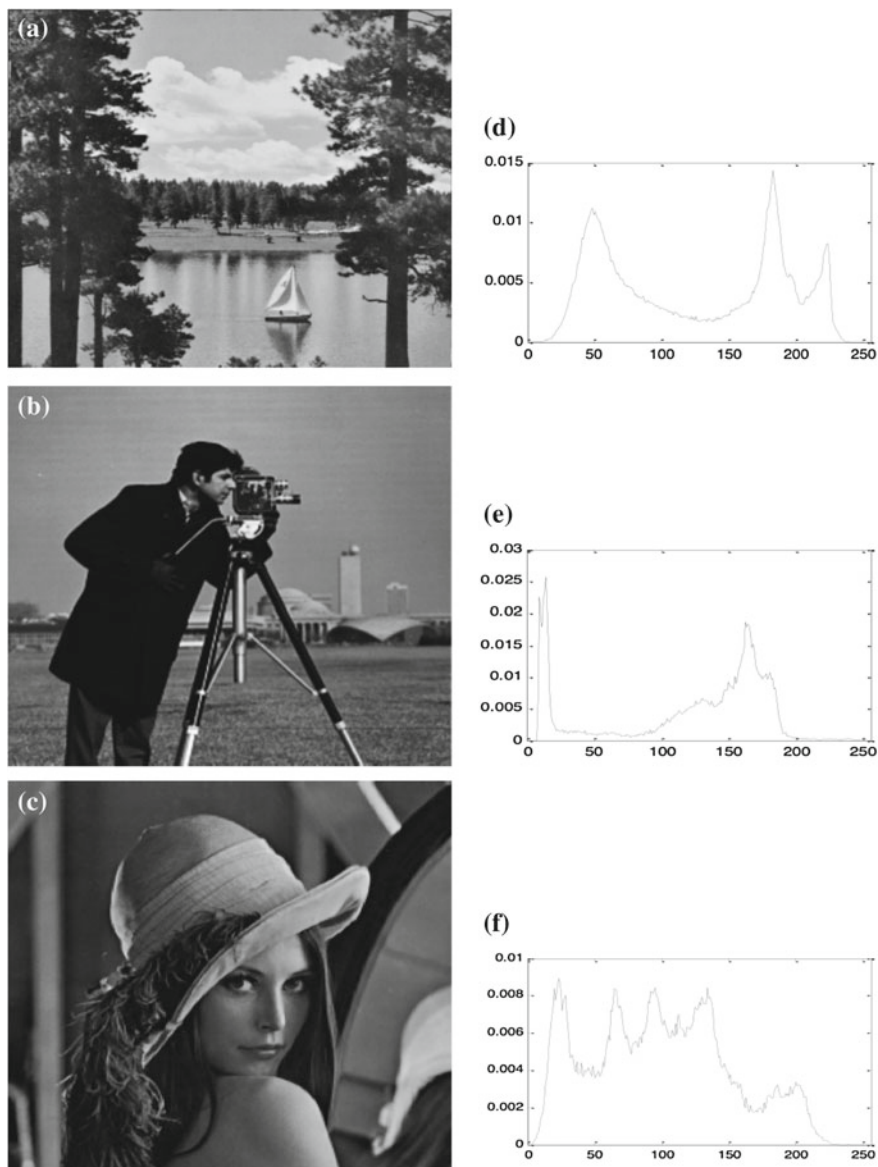


**Fig. 2.1** Test images and their normalized histograms. **a** Sailboat, **b** Cameraman, **c** Lena, **d** histogram of Sailboat image, **e** histogram of Cameraman image and **f** histogram of Lena image

**Table 2.1** Parameters of HDE.  $nc = 3 - D$ , where D is the number of segmentation classes (to be fixed by the user)

Parameter	Value
Population size $NP$	$10 \times N$
Scaling factor $F$	0.25
Crossover rate $C_r$	0.20
Maximum iteration	200

**Table 2.2** Comparison of HDE with basic DE in terms of CPU time and NFE

Images	No. of Classes	DE		HDE	
		Time	NFE	Time	NFE
Silboat	3	5.9143	17280	5.8968	10110
	4	9.6739	23280	9.2041	1630
Camera man	3	5.8034	16740	5.7876	10320
	4	9.0024	22920	8.8609	16090
	3	5.9675	17010	5.8968	11270
Lena	5	12.934	27750	12.8077	18300
	5	5			

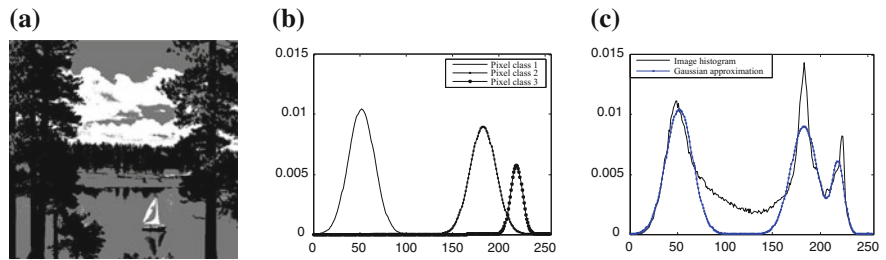


**Fig. 2.2** Results of Sailboat image with three classes: **a** segmented image, **b** Gaussian function of each class and **c** original histogram and corresponding Gaussian approximation

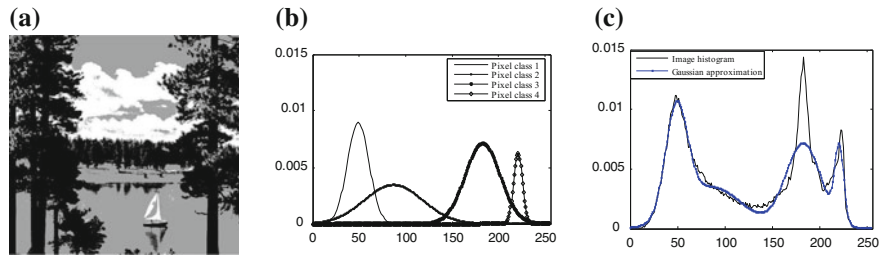


**Fig. 2.3** Results of Sailboat image with four classes: **a** segmented image, **b** Gaussian function of each class and **c** original histogram and corresponding Gaussian approximation



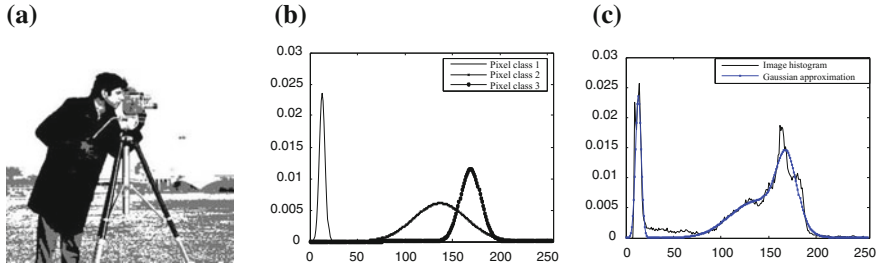


**Fig. 2.4** Results of Cameraman image with three classes: **a** segmented image, **b** Gaussian function of each class and **c** original histogram and corresponding Gaussian approximation

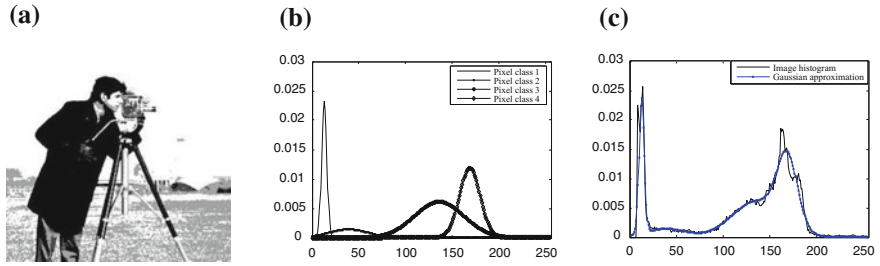


**Fig. 2.5** Results of Cameraman image with four classes: **a** segmented image, **b** Gaussian function of each class and **c** original histogram and corresponding Gaussian approximation

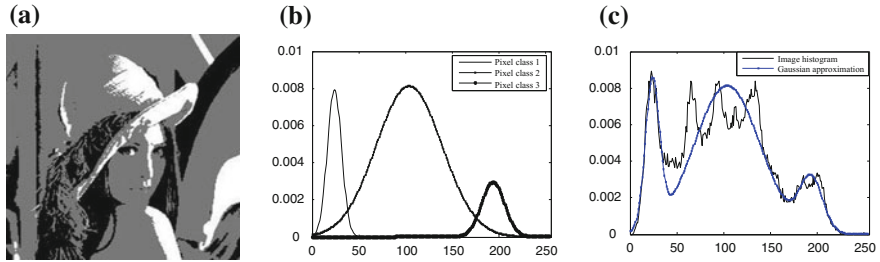


**Fig. 2.6** Results of Lena image with three classes: **a** segmented image, **b** Gaussian function of each class and **c** original histogram and corresponding Gaussian approximation

To further quantitatively judge the quality of the algorithm with several other thresholding-based segmentation algorithms [12], the uniformity measure is utilized which has also been extensively used in the literature. This uniformity measure is given by:

$$U = 1 - 2 \times (nc - 1) \times \frac{\sum_{j=0}^{nc-1} \sum_{i \in R_j} (f_i - m_j)^2}{N \times (f_{max} - f_{min})} \quad (2.14)$$

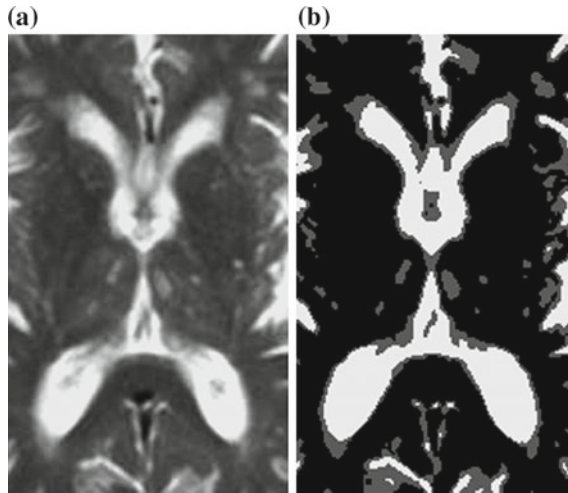


**Fig. 2.7** Segmentation of brain MRI of the ventricles. **a** Original slice, **b** Segmented slide into 3 classes,  $t = (134; 187)$

where,  $nc$  denotes number of classes,  $R_j$  denotes the  $j^{th}$  segmented region,  $f_i$  indicates the gray level of the pixel  $i$ ,  $m_j$  mean gray level of pixels in  $j^{th}$  region,  $N$  denotes the total number of thresholds in the given image,  $f_{max}$  gives the maximum gray level of pixels in the given image and  $f_{min}$  gives minimum gray level of pixels in the given image.

The value of the uniformity measure,  $U$ , should be a positive fraction i.e. it should lie between 0 and 1. A higher value of  $U$  indicates that there is better uniformity in the thresholded image, depicting better quality of thresholding and vice versa. It can be also seen from Table 2.4 that the proposed HDE algorithm could achieve significantly better segmentation results as demonstrated by its higher values of  $U$  in each case, compared to other methods

In order to analyze the obtained results from statistical point of view, we do a Wilcoxon test. Then, the p-value obtained from the results of Table 2.4 is equal to 0.0152 that indicates a significant different between the original DE and the enhanced DE.

## 2.6 MRI Slices Segmentation

Magnetic resonance imaging (MRI) is a medical imaging technique used in radiology to image the anatomy and the physiological processes of the body in both health and disease. MRI devices or scanners are based on strong magnetic fields, radio waves, and field gradients to form images of the body.

**Table 2.3** Results obtained by HDE for images given in Fig. 2.1

Image	Size(in number of pixels)	Number of classes	Parameters of Gaussian approximations	Time (s)	Threshold
Sailboat	512 × 512	3	$P(0.0102, 0.0078, 0.0065)$	5.8968	117,205
			$\mu(53, 182, 221)$		
			$\sigma(21.8457, 24.9995, 7.0544)$		
		4	$P(0.0090, 0.0035, 0.0071, 0.0062)$	9.2041	95,121,205
			$\mu(49,87,183,221)$		
			$\sigma(16.4485, 44.4340, 26.5073, 6.6560)$		
Cameraman	256 × 256	3	$P(0.0235, 0.0061, 0.0114)$	5.7876	33,130
			$\mu(13, 137, 169)$		
			$\sigma(4.3845, 39.2224, 15.4275)$		
		4	$P(0.0231, 0.0014, 0.0061, 0.0118)$	8.8609	30,52,131
			$\mu(13, 39, 136, 169)$		
			$\sigma(3.9712, 29.6954, 37.0420, 15.5644)$		
Lena	256 × 256	3	$P(0.0079, 0.0081, 0.0029)$	5.8968	53,170
			$\mu(24, 104, 194)$		
			$\sigma(10.7663, 49.9796, 17.4342)$		
		5	$P(0.0084, 0.0070, 0.0066, 0.0074, 0.0032)$	12.8077	46, 80, 114,176
			$\mu(25, 63, 94, 131, 191)$		
			$\sigma(12.1269, 15.6615, 16.0053, 23.8994, 22.1594)$		

Since its early development in the 1970s and 1980s, MRI has proven to be a highly versatile imaging technique. While MRI is most prominently used in diagnostic medicine and biomedical research, it can also be used to form images of non-living objects. MRIs are able to produce a variety of chemical and physical data, in addition to detailed spatial images.

MRI is widely used in hospitals and clinics for medical diagnosis, staging of disease and follow-up without exposing the body to ionizing radiation. For our work, the data were from the CHU Henri Mondor, Créteil (France).

**Table 2.4** Comparison of HDE with basic PSO and GA

Image	No. of classes	Threshold			Uniformity measure		
		PSO	GA	EDE	PSO	GA	EDE
Sailboat	3	96,201	89,210	117,205	0.9632	0.9535	0.9697
	4	90, 115, 208	88, 115, 205	95, 121, 205	0.9664	0.9681	0.9694
Camera man	3	30, 135	30, 142	33, 130	0.9752	0.9744	0.9764
	4	28, 48, 145	28, 50, 145	30, 52, 131	0.9735	0.9732	0.9736
Lena	3	61, 166	53, 178	53, 170	0.9597	0.9490	0.9533
	5	46,84, 119, 186	46, 77, 115, 186	46, 80, 114, 176	0.9774	0.9758	0.9807

MRI has a wide range of applications in medical diagnosis and over 25000 scanners are estimated to be in use worldwide. MRI affects diagnosis and treatment in many specialties although the effect on improved health outcomes is uncertain. Since MRI does not use any ionizing radiation, its use is generally favored in preference to CT when either modality could yield the same information. For all these reasons developing tools for analysis these data is very important.

To illustrate the performance of our segmentation algorithm for the analysis of CT-Scan images. Two examples are presented in Figs. 2.7 and 2.8. In the first example, the region of interest was the ventricles and the goal was to extract the segment the

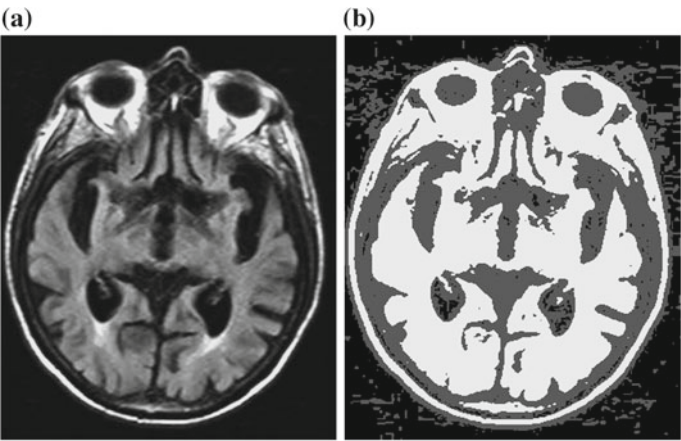


**Fig. 2.8** Illustration of the Segmentation of a retinal angiography image where the goal is to extract drusens. **a** Original pathologic Image, **b** Original histogram and its approximation, **c** Segmentation on 2 classes,  $t = 150$

ventricular system represented by high intensity voxels. In this case, the presented results consists in a segmentation on 3 classes to have more accuracy.

The second example presented here

## 2.7 Conclusions

In this paper, a modified DE algorithm namely HDE, is used for image segmentation. The objects and background components within the image are assumed to fit into Gaussian distributions exhibiting non-equal means and standard deviations. The histogram can thus be approximated by a mix of Gaussian probability functions. The algorithm HDE is used to estimate the parameters for the mixing density function as it seeks to get a minimum error between the density function and the original histogram. Experimental results show that HDE produces satisfactory results, indicating that it can be used for image segmentation in multi-thresholding due to its computational efficiency. Additionally, HDE appears to be effective due to its quality performance. The proposed work can easily be extended in several directions. In the future we intend to perform a formal comparison with other state-of-the-art image segmentation techniques and also we will take a wider range of test images.

## References

1. A. Baxsturk, E. Gnay, Efficient edge detection in digital images using a cellular neural network optimized by differential evolution algorithm. *Expert Syst. with Appl.* **36**(2), 26452650 (2009)
2. A.K. Bhandari, A. Kumar, G.K. Singh, Tsallis entropy based multilevel thresholding for colored satellite image segmentation using evolutionary algorithms. *Expert Syst. with Appl.* **42**(22), 8707–8730 (2015)
3. A. Bouaziz, A. Draa, S. Chikhi, Artificial bees for multilevel thresholding of iris images. *Swarm Evolut. Comput.* **21**, 32–40 (2015)
4. P. Bratley, B.L. Fox, ALGORITHM 659 implementing Sobol's Quasi random sequence generator. *ACM Trans. Math.Softw.* **14**(1), 88–100 (1988)
5. W.-D. Chang, Parameter identification of Rosslers chaotic system by an evolutionary algorithm. *Chaos, Solitons & Fractals* **29**(5), 1047–1053 (2006)
6. E. Cuevas, D. Zaldivar, M. Prez-Cisneros, A novel multi-threshold segmentation approach based on differential evolution optimization. *Expert Syst. Appl.* **37**(7), 265–5271 (2010)
7. S.-K.S. Fan, Y. Lin, A multi-level thresholding approach using a hybrid optimal estimation algorithms. *Pattern Recognit. Lett.* **28**, 662–669 (2007)
8. R.C. Gonzalez, R.E. Woods, *Digital Image Processing* (Prentice Hall, Upper Saddle River, 2002). N. Otsu, A threshold selection method for gray-level histogram. *IEEE Trans. Syst. Man Cybernet* **9**, 62–66 (1979)
9. B. Liu, L. Wang, Y.-H. Jin, D.-X. Huang, F. Tang, Control and synchronization of chaotic systems by differential evolution algorithm. *Chaos, Solitons & Fractals* **34**(2), 412419 (2007)
10. A. Nakib, H. Oulhadj, P. Siarry, Image histogram thresholding based on multiobjective optimization. *Signal Process.* **87**, 2516–2534 (2007)
11. A. Nakib, H. Oulhadj, P. Siarry, Non supervised image segmentation based on multiobjective optimization. *Pattern Recognit. Lett.* **29**, 161–172 (2008)

12. P.D. Sathya, R. Kayalvizhi, Development of a new optimal multilevel thresholding using improved particle swarm optimization algorithm for image segmentation. *Int. J. Electron. Eng.* **2**(1), 63–67 (2010)
13. M. Sezgin, B. Sankur, Survey over image thresholding techniques and quantitative performance evaluation. *J. Electron. Imaging* **13**(1), 146165 (2004)
14. R. Storn, K. Price, Differential evolution a simple and efficient adaptive scheme for global optimization over continuous spaces, Technical Report TR-95-012, Berkeley, CA (1995)
15. R. Storn, K. Price, Differential evolution a simple and efficient heuristic for global optimization over continuous spaces. *J. Global Optim.* **11**(4), 341–359 (1997)
16. W. Synder, G. Bilbro, A. Logenthiran, S. Rajala, Optimal thresholding-a new approach. *Pattern Recognit. Lett.* **11**, 803–810 (1990)
17. J. Vesterstrom, R. Thomsen, A comparative study of differential evolution, particle swarm optimization and evolutionary algorithms on numerical benchmark problems, in *Proceedings of the Congress on Evolutionary Computation 2004 (CEC2004)*, vol. 2, Portland, Oregon, 20–23 June 2004, pp. 1980–1987
18. J.S. Weszka, R. Azriel, Histogram modifications for threshold selection. *IEEE Trans. Syst. Man Cybern.* **9**(1), 38–52 (1979)
19. E. Zahara, S.-K.S. Fan, D.-M. Tsai, Optimal multi-thresholding using a hybrid optimization approach. *Pattern Recognit. Lett.* **26**, 1082–1095 (2005)

Metaheuristics for Medicine and Biology

Nakib, A.; Talbi, E.-G. (Eds.)

2017, XVIII, 211 p. 120 illus., 67 illus. in color.,

Hardcover

ISBN: 978-3-662-54426-6